Design, Fabrication & Testing of a Low-Power Electric Thruster for Nanosatellite Missions

Zoë Jaeger-Letts

***Abstract*—Low-power electric propulsion technology is considered essential for the realisation of ambitious nanosatellite missions. By operating in a low-power regime, miniaturised electric thrusters can be used to propel nanosatellites and other small spacecraft, providing the unique opportunity for missions with advanced manoeuvres. Inspection of literature highlighted a distinct lack of efficient and reliable low-power electric thrusters that can support such missions. Furthermore, the consequences of scaling electric thrusters down to the sub-100 W power regime is not yet well understood.**

A novel low-power Hall-effect thruster and hollow cathode were designed, fabricated, and tested. Finite element analysis methods were used to simulate magnetic field patterns and understand their influence on thruster performance and stability. A parametric sweep during testing identified the mass flow rate as well as discharge current and voltage as key parameters for varying performance. The analysis focuses on the thruster's performance using standard metrics such as thrust and specific impulse, with an additional focus on observing the thruster's stability through different operating regimes.

A characterisation of the hollow cathode identified a stable low-power operating regime that could be reached routinely. A repeatable measurement of 3 mN was achieved with the cathode operating at $\mathbf{I_c = 0.6\,A}$ and $\mathbf{\dot{m}_c = 4\,mg/s}$, and the anode operating at $\mathbf{I_a = 0.2\,A}$ and $\mathbf{\dot{m}_a = 10\,mg/s}$.

***Index Terms*—Electric propulsion; satellite; nanosatellite; electromagnetic; electrostatic; low power; Hall thruster.**

I. Introduction

SELF-PROPELLED small spacecraft are driving a revolution in space exploration. Miniaturised space technology, such as nanosatellites [1], allows more cost-effective and sustainable space exploration, as well as opening up new avenues for scientific enquiry and discovery [1].

In the past, small satellites have been limited to passive, Low Earth Orbit (LEO) missions due to the stringent mass, volumetric, and power budgets imposed by compact form factors and payload launch requirements. The development of reliable and efficient microelectronics and miniaturised electric propulsion (EP) thrusters is required to fully realise ambitious and long-duration self-propelled nanosatellite missions [2] [3]. Such missions enable the collection of invaluable scientific data over extended periods and orbital regions, as well as the deployment of satellite constellations. These networks have far-reaching benefits, from climate research and astronomical observations, borderless access to the internet, and fostering a deeper understanding of our planet and space.

A 3U CubeSat [2] mission is proposed the Victoria University of Wellington (VUW) School of Engineering and Computer Science (ECS) in collaboration with Robinson Research Institute (RRI) [4]. The mission involves launching the CubeSat into a temporary LEO, where it engages in a constant burn, propelling itself with 2 mN of thrust into Geostationary Orbit (GEO) over approximately 100 days. During this time, the CubeSat will collect in-orbit measurements of Earth's magnetic field at increasing altitudes. This mission relies firmly on the development of a novel low-power solar-electric powered micropropulsion system that can meet the specifications stated.

Inspection of EP literature highlighted a distinct lack of understanding and development work on compact low-power[3] miniaturised electric thruster technology. Thrusters with input powers of several hundred watts have received significant attention in the field [3] [1]. However, very few thrusters operating in sub-100 W regimes have been developed and tested. Furthermore, the impact that scaling EP thrusters down to the sub-100 W range has on their operation and performance has not been comprehensively explored. Consequently, there is an absence of efficient and reliable electric thruster designs that can support ambitious nanosatellite missions.

A low-power EP thruster was designed to meet the mission specifications of the self-propelled CubeSat mission proposed by VUW. This paper presents a fast-tracked Hall-effect thruster (HET) design and testing framework, with a focus on thruster scaling and design decisions required for thruster implementation. Although the development of a thruster is crucial for the VUW mission, the principal aim of the project is to build knowledge around the engineering aspects of the design and evaluation of miniaturised thrusters.

Testing focused on characterising the electrical behaviour of the hollow cathode and the HET. Thrust measurements from a torsional thrust stand are also presented. The data gathered enables a quantitative evaluation of the thruster's performance against standard propulsion metrics like thrust, total efficiency, and specific impulse. **These project goals are summarised below:**

1) Identify a suitable thruster technology that could feasibly support the proposed 3U CubeSat mission.
2) Investigate the underlying relationships between thruster operating parameters and simulate key thruster subsystems (like the magnetic configuration) to verify understanding and inform design decisions.

This project was supervised by Dr. Jakub Głowacki (Robinson Research Institute) and Dr. Christopher Hollitt.

[1] Satellites between 1-10 kg

[2] A 30x10x10 cm nanosatellite

[3] Thrusters that require between 1 and 200 W of input electrical power are defined as low-power [5] [6]

3) Design the mechanical construction of the scaled thruster and create computer-aided design (CAD) models for part fabrication using the principles discovered in the above step.
4) Characterise the thruster to build an understanding of the impact that thruster scaling and key operational parameters, such as mass flow rate, current, and voltage, have on the performance of the thruster. This will include testing the thruster in the large vacuum chamber at RRI.

A. Electric Propulsion Theory

In-space EP encompasses any propulsion technology wherein electrical energy is converted to kinetic energy to propel a spacecraft [2]. While electric thrusters have many figures of merit, thrust, specific impulse, and thruster efficiency are of primary interest for mission planners [7]. As such, these three parameters define the initial design constraints for a thruster intended for a defined mission.

$$T = \dot{m}\, v_{\mathrm{ex}} \tag{1}$$

$$I_{\mathrm{sp}} = \frac{v_{\mathrm{ex}}}{g_0}. \tag{2}$$

$$\eta = \frac{P_{\mathrm{jet}}}{P_{\mathrm{in}}} = \frac{T^2}{2\,\dot{m}\,P_{\mathrm{in}}} \tag{3}$$

where T is thrust, $\dot{m}$ is the mass flow rate of propellant, v_{ex} is the exhaust velocity, I_{sp}, is specific impulse, g_0 is the standard gravitation constant ($9.81\mathrm{m/s^2}$), η is total thruster efficiency, P_{jet} is the kinetic (jet) power, and P_{in} is the input electrical power.

1) Thrust: EP devices generate thrust using the same mechanism as traditional chemical rockets – accelerating mass and ejecting it from the spacecraft [8]. The equation for thrust, given by (1), is derived by applying Newton's second law of motion and conserving the momentum of the spacecraft:

$$m(t)\,\frac{dv}{dt} = v_{\mathrm{ex}}\,\frac{dm_{\mathrm{p}}}{dt} \tag{4}$$

where $m(t)$ is the spacecraft mass at a given time, t, the spacecraft's velocity is denoted v, and m and m_{p} are the total mass of the spacecraft and the mass of propellant on-board, respectively.

2) Specific Impulse: Specific impulse is a measure of how efficiently a thruster produces a net change in velocity, and is given by the ratio described in (2). Commonly referred to as the ideal rocket equation, (5), highlights the crucial function that specific impulse plays in leveraging thruster performance [9].

$$\Delta v = I_{\mathrm{sp}}\, g_0\, \ln\!\left(\frac{m_0}{m_{\mathrm{f}}}\right) = v_{\mathrm{ex}}\, \ln\!\left(\frac{m_0}{m_{\mathrm{f}}}\right) \tag{5}$$

where Δv is delta-*v* (an increment in spacecraft velocity), and m_0 and m_{f} are the spacecraft's initial and final burnout masses respectively [4]. Since delta-*v* indicates roughly how far a spacecraft can travel for a specified thruster and propellant mass, maximising it is often a priority in mission analysis. Where the exhaust velocity of a chemical rocket is inherently limited by the energy contained in the propellant, electric thrusters rely on external power sources (solar panels or nuclear reactors) for energy and can therefore achieve much higher exhaust velocities. By achieving higher specific impulse and exhaust velocities, electric thrusters can decrease the amount of propellant needed to achieve mission objectives, which is shown in (5). This feature of EP makes it preferable for small spacecraft which cannot host large amounts of propellant on board due to their volumetric and mass constraints.

3) Thruster Efficiency: The overall efficiency of any electrically powered thruster is given by (3). There are several power-loss mechanisms in electric thrusters, including incomplete neutral gas ionisation and electrical input losses [10]. An effective EP device maximises efficiency to minimise the input power required to produce a specified thrust. Maximising efficiency also reduces the amount of waste heat that the system must dissipate. Considering heat transfer in a vacuum is limited to two mechanisms; conductive and radiative transfer, dealing with waste heat is a non-trivial challenge. This makes the development of highly efficient thrusters crucial to preventing thruster malfunction and thermal soak-back to the spacecraft from the thruster.

B. Sustainability in Space

This project has integrated ideas of engineering sustainability by considering the human, social, economic, and environmental impacts of this project.

Following the design trend of miniaturisation seen in the space industry today, this project focuses on creating a small-scale thruster. Miniaturisation of technology promotes the development of experimental technology that uses less monetary and material resources than larger-scale engineering projects. The small-scale of this project also ensures that if the future launch is unsuccessful, there will be less space junk flying around in LEO. National Aeronautics and Space Administration (NASA) identifies even the smallest pieces of space debris as a source of "potential danger to all space vehicles, including the International Space Station and other spacecraft with humans aboard" [11].

Furthermore, this project recognises the use of certain scarce materials, such as xenon gas, as being in high demand by many other industries and difficult to extract [12]. Therefore, only alternative gases that are easier to extract (such as argon) were considered for use as a propellant to minimise the carbon footprint of the project, as well as to ensure that limited resources are not pulled from other industries that rely on them.

Chemical propulsion necessitates the utilisation of propellants such as hydrazine, a highly toxic and reactive propellant that is at risk of being banned in Europe [13]. Electric propulsion does not rely on the combustion of propellants, therefore safe, chemically inert, and "green" propellants can be used, which do not pose the same risks to living organisms and the environment.

II. Background & Previous Work

Given the mass, power, and operational constraints of small satellite missions, not all types of EP can be employed, and

[4] $\frac{m_0}{m_{\mathrm{f}}}$ is often referred to as a spacecraft's mass fraction.

few technologies have actually been flown in space with successful results [14]. Therefore, the selection of thruster technology was a crucial design decision for the project and was informed by a review of the literature on thruster technologies.

A. Review of Existing Technologies

Electric thrusters are generally classified as electrothermal, electrostatic, or electromagnetic, according to their principle of operation [2]. While EP was first postulated in the early 20th Century by rocket science pioneers Robert Goddard, Konstantin Tsiolkovsky, and Hermann Oberth [7], the first operational electric thrusters were not flown until the 1960s. Their crude technology and inefficient spacecraft electronics of the time limited their applications to attitude control and other minor manoeuvres [12]. The testing of these early thrusters established the need for more efficient EP electric propulsion systems to be considered as an alternative to chemical propellant. The long-standing EP technologies developed during this time include HET (electrostatic) and resistojets (electrothermal) [15].

The end of the 20th Century saw a significant increase in EP efficiency with the advent of thrusters operating at higher specific impulses than previously conceivable. The development of successful thrusters such as the SPT-100 HET [16] [15], the XIPS-25 ion thruster, and the PPS-1350 HET[5] demonstrated that EP thrusters could achieve efficiencies exceeding 50% [16]. However, despite their high efficiencies, these thrusters required input powers in the kilowatt range, which cannot be supplied by smaller satellite platforms due to the inherent volumetric and mass constraints they impose. The challenge with adapting EP thrusters for smaller platforms lies in scaling down their dimensions while preserving high efficiencies [1].

A review of commercially available thrusters (summarised in Figure 1) identified a lack of thrusters that can operate within the regime of interest specified by the proposed VUW mission, indicating the novelty of reliable high-performance nanosatellite propulsion.

Fig. 2 summarises a study on the various theoretical operating regimes of different EP technologies [15]. The operating regime called for by the 3U VUW mission, (thrust-to-power ratio (TPR) of 66 mN/kW, and specific impulse between 1000 and 2000 s) is indicated by the red box. Reading the plot, it is clear to see that there are only two technologies that operate within this regime; self-field magnetoplasmadynamic thruster (SF-MPDT) and HET. Therefore, the technology selection for this project was narrowed down to between these two technologies.

An SF-MPDT is a type of electromagnetic thruster that generates thrust by ionising a gaseous propellant and accelerates it using electric and induced magnetic fields. SF-MPDTs are considered advantageous because they have high propulsive power, but are generally not scaled below 1 kW as their performance drops steeply [1]. However, multiple-stage operation has proven to negate this feature of SF-MPDTs.

[5]The thruster that took the 367 kg SMART-1 European Space Agency (ESA) satellite from GEO to the Moon in 2003 [16].

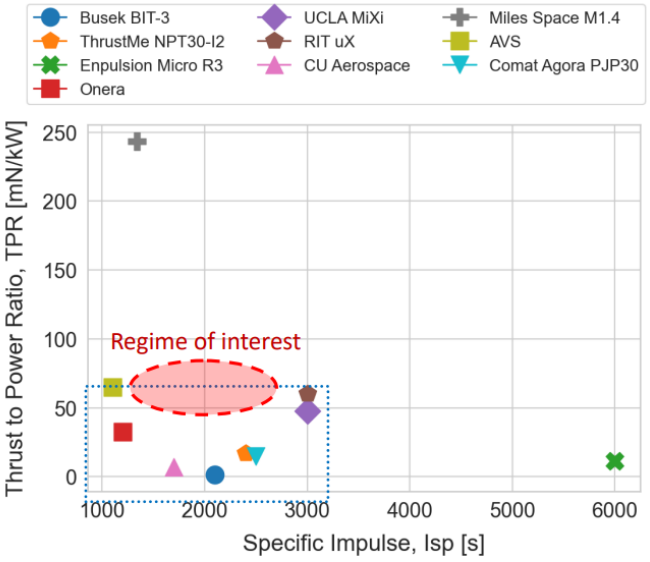

Fig. 1: Collated research on commercial thrusters from [4]

A thruster designed at George Washington University [17] achieved stable operation with 1.7 mN of thrust from under 50 W of input power, operating with 50 % efficiency. Their results showed that the thrust measurements increased by three orders of magnitude with the second-stage voltage, indicating the effectiveness of the thruster's second ionisation stage. This type of thruster design is highly novel, and the implementation of second ionisation stages introduces many complexities with design and testing facilities; therefore, the development of a similar SF-MPDT would be outside the scope of this project.

The HET has a long and successful flight history for both large- and medium-scale propulsion systems, indicating the reliability and robustness of the scalability of the technology [2]. NASA have specifically selected HETs for use in future missions on their Technology Roadmap, and several publications identify HET as the most promising technology for low-power applications due to their high efficiencies and high thrust-to-power ratio. [2] [1] [3].

Sub-100 W HETs are still novel and only a few systems have been evaluated in literature. A 50 W HET developed in South Korea successfully demonstrated a TPR of 50 mN/kW, but could not produce a magnetic field strong enough with their permanent magnet arrangement and thruster geometry [18]. An 85 W HET developed at the Japan Tokyo Metropolitan University of Japan with Japan Aerospace Exploration Agency (JAXA) demonstrated similar performance, achieving a TPR of 59.5 mN/kW and specific impulse of 1050 s [19]. However, the study failed to characterise the behaviour of its thruster under different magnetic circuit designs and mass flow rate regimes which is required for validating the designed operating regime and measurements gathered [20]. A low-power HET and hollow cathode developed in Germany at the Technical University of Dresden achieved stable operation across a 5 W to 150 W operating regime [20]. However, their analysis is set short by a lack of thrust measurements, which is crucial to quantifyi ng the performance of EP thrusters. These recent studies encountered several thematic challenges while

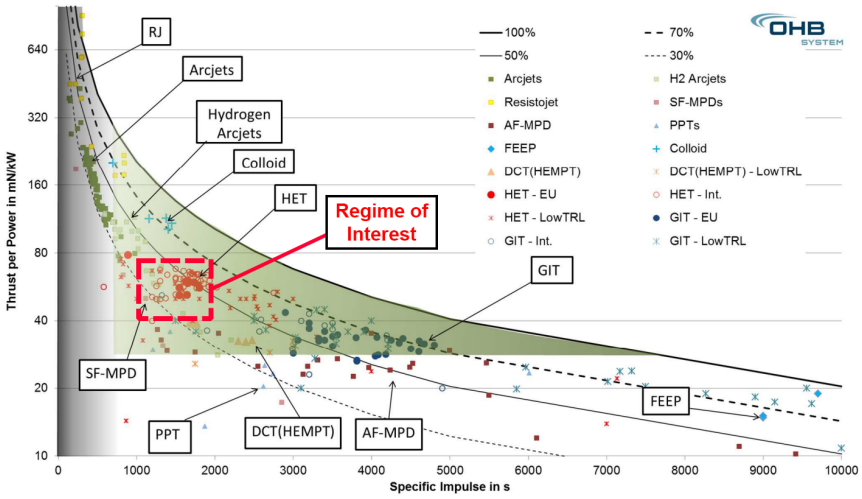

Fig. 2: OHB Propulsion review of thruster technologies and their operating regimes [15].

scaling down thrusters to sub-100 W sizes, which set their findings short. These challenges were:

1) Providing a sufficiently strong magnetic field while meeting low-power and low-mass constraints.
2) Ensuring reliable low-power cathode ignition and operation.
3) Measuring minute thrust forces.

A comprehensive study of the influence of thruster operational parameters is required for finding a balance in the trade-off between operating regimes, thruster dimensions, thrust output, and power requirements.

III. Design

The design methodology used in this project follows an established thruster design procedure whereby initial design decisions are informed by semi-empirical formulation extracted from databases of previously tested thrusters [21] [22] [23]. The scaling laws derived from these represent relationships between key operating parameters and are often corrected to fit the required operational regime, forming guidelines on how a thruster should be sized.

This methodology was selected for several reasons. First, it leverages a well-informed design start-point based on real operational data, adding reliability and predictability to an otherwise nontrivial design process and maximising collective knowledge from the field. It also expedites the design process; by limiting the requirement for theoretical calculations and simulations that other thruster sizing methodologies require, this semi-empirical approach provides a time-saving sizing method. This makes the semi-empirical methodology an extremely powerful design tool from an engineering perspective. One downside to this approach is that it detaches the design process from the first principles physics of the thruster, thus limiting the accuracy of the scaling parameters. However, a verification method can be used to probe the accuracy of the resultant scaling parameter values.

A. Thruster Operating Theory & Architecture

To apply scaling laws, a foundational understanding of HET principles is required. In Hall thrusters, a radial magnetic field (shown as blue lines in Fig. 3) reduces the axial mobility of the electrons travelling from the hollow cathode to the anode. The electrons are subject to an $\vec{E} \times \vec{B}$ Lorentz force, resulting in the generation of a Hall-effect current. This force compels electrons to spiral along the magnetic field lines where they gyrate with a Larmor radius denoted r_{e} and a velocity of v in the $\vec{E} \times \vec{B}$ direction. This velocity is given by (6):

$$\vec{v} = \frac{\vec{E} \times \vec{B}}{|B|} \tag{6}$$

where $\vec{E} \times \vec{B}$ is the cross product of the electric and magnetic fields, and $\vec{B}$ is the strength of the magnetic field at the opening of the thruster channel. Circulating electrons require a certain velocity to remain captured in the magnetic lens. Once they eventually lose energy from collisions with propellant neutrals or channel walls, they travel to the anode and re-enter the circuit [24].

Electrons bombard and ionise neutral propellant particles injected to the channel through the anode. This produces ions in a plasma volume [6] which are accelerated by the application of an axial electric field (shown in green in Fig. 3) across the discharge chamber [3]. It is important to note that the plasma maintains quasineutrality, whereby the electron plasma density, n_{e}, and ion plasma density, n_{i}, are approximately equal ($qn_{\mathrm{e}} \approx qn_{\mathrm{i}}$) [7]. Quasineutrality defines a state of approximate equilibrium where the plasma returns to by either pulling back or expelling charges. The consequence of this is that the thruster's ion beam must be neutralised by electrons from the cathode to avoid the ion being pulled back towards the thruster [24]. This would result in the negation of the momentum gained by having fired the ions, and no net force being applied to the thruster.

[6]Plasma is ionised gas, which is fundamentally a collection of electrons or ions free to move in response to generated or applied fields [7].

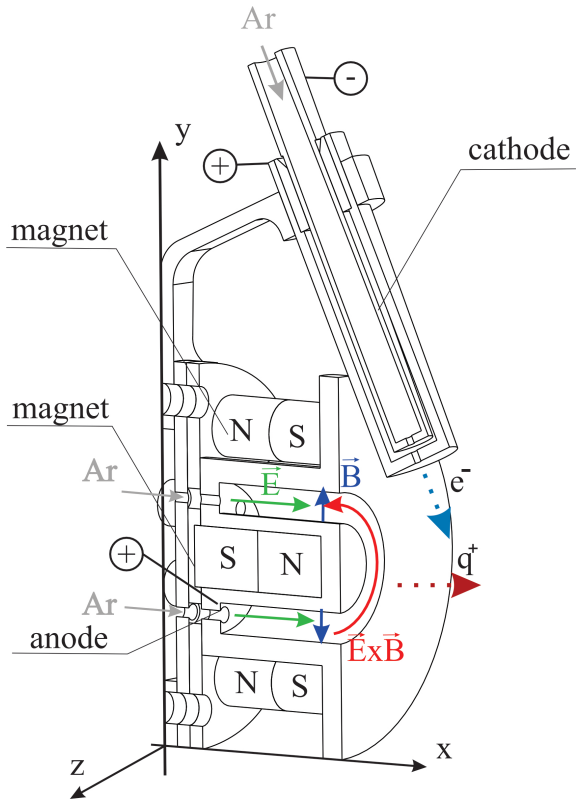

Fig. 3: Cross-sectional schematic of the thruster showing the main components as well as the magnetic and electric fields, and $\vec{E} \times \vec{B}$ drift

There are three key sub-systems in the artefact HET's architecture:

1) **The thruster body** which consists of an annular body with a discharge channel and an interior copper anode.
2) **A magnetic circuit** that can produce a magnetic field with a specified intensity.
3) **An externally mounted cathode** for propellant ionisation and beam neutralisation.

B. Thruster Scaling

Ensuring the successful operation of HETs is based on correct size of the thruster. This requires that several common scaling laws in the literature be satisfied [7]. These laws are as follows:

1) **Ionisation and Plasma Containment:** To ensure a sufficient ionisation of the propellant gas, the moving atoms must stay inside the channel for long enough. This requires that the Melikov-Morozov criterion is satisfied [21]:

$$\lambda_\mathrm{i} = \frac{v_\mathrm{n}}{n_\mathrm{n}\,\sigma_\mathrm{i}\,v_\mathrm{e}\,T_\mathrm{e}} \ll L \tag{7}$$

where λ_i is the ionisation mean free path[7], v_n and n_n are the velocity and number of neutral particles in the chamber, respectively, σ_i is the cross-sectional area of ionisation, v_e and T_e are the velocity and temperature of electrons in the chamber, respectively, and L is the channel length.

2) **Electron Confinement:** The magnetic field strength in a HET must be such that electrons are trapped axially and ions are not (so they can be accelerated). For this to hold, the following criterion must be fulfilled:

$$r_\mathrm{e} \ll L \ll r_\mathrm{i} \tag{8}$$

where:

$$r_\mathrm{e} = \frac{1}{B}\sqrt{\frac{8\,m_\mathrm{e}\,k\,T_\mathrm{e}}{\pi\,e}} \tag{9}$$

$$r_\mathrm{i} = \frac{1}{B}\sqrt{\frac{2\,m_\mathrm{i}\,V_\mathrm{d}}{e}} \tag{10}$$

are the electron and ion Larmor radii respectively, and m_e is the mass of an electron, m_i is the mass of a propellant ion, k is the Boltzmann constant ($8.62 \times 10^{-5}\,\mathrm{eV/K}$), and T_e is the electron temperature, e is the elementary charge $1.60 \times 10^{-19}\,\mathrm{C}$, and V_d is the discharge voltage.

There are three characteristic dimensions for thruster sizing: channel length, L, channel width, w, and channel mean diameter, $d = \frac{1}{2}(d_\mathrm{ex} + d_\mathrm{int})$, where d_ex and d_int are the external and interal diameters of the thruster, respectively. The approximate values for the electron and ion Larmor radii can be calculated using (9) and (10) by assuming an electron temperature of 40 eV and a magnetic field of 0.02 T[8], and given that the mass of an argon ion is $6.63 \times 10^{-26}\,\mathrm{kg}$. This calculation yields $r_\mathrm{e} = 2.13\,\mathrm{mm}$ and $r_i = 45.49\,\mathrm{mm}$. Taking into account the electron confinement criterion (8), the limits for the thruster channel length can therefore be established as $2.13\,\mathrm{mm} \ll L \ll 45.49\,\mathrm{mm}$.

Several studies have demonstrated proportionality between anode flow rate and the annular channel area[9] ($\dot{m}_\mathrm{a} \propto wd$), as well as between channel width and mean diameter ($w \propto d$) [21] [25]. Two linear relations can be derived:

$$\dot{m}_\mathrm{a} = C_1\,wd \tag{11}$$

$$w = C_2\,d \tag{12}$$

where C_1 and C_2 are proportionality constants. The values of these constants can be approximated by fitting a linear regression line to the data from the thruster database and calculating the slope of the line. Fig. 4 *b)* shows a line fit to the thruster data with an equation of $\dot{m}_\mathrm{a} = 0.0036\,wd$. Therefore, $C_1 \approx 0.0036$ and $C_2 \approx 0.2172$. The initial target for the anode mass flow rate was 0.5 mg/s. Applying the proportionality relation gives $wd = 138.89\,\mathrm{mm}^2$. Fig. 4 *a)* has a regression line fit by $w = 0.2172\,d$, which allows for the derivation of w and d individually, yielding 25.29 mm and 5.493 mm, respectively.

When the mass flow rate is assumed to be fixed, the length of the channel, L, is a function of the magnetic field strength, $\vec{B}$ [21]. This relationship highlights an inherent problem with scaling down electric thrusters to operate in low-power

[7]The ionisation mean free path is the average distance travelled by a moving particle before it collides with another particle or the channel wall [7].

[8]These assumptions were made based on values from similar thrusters described in literature.

[9]The product of channel width and mean diameter.

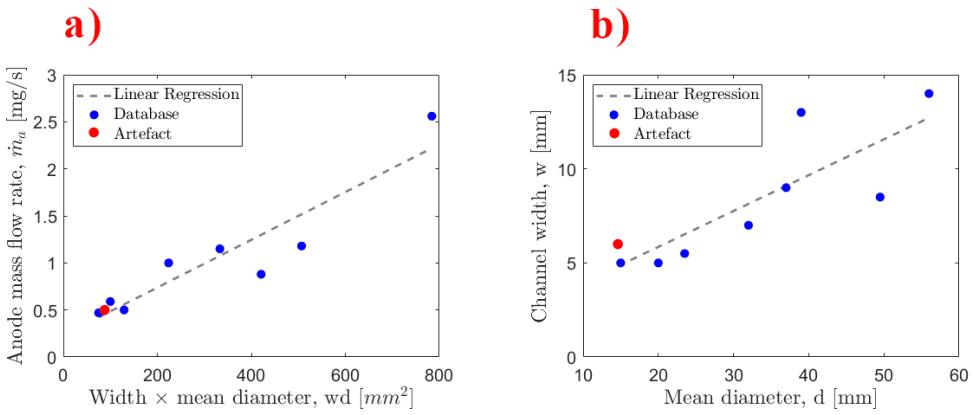

Fig. 4: *a)* Mean diameter as a function of thruster channel width, assessed for the thrusters in the scaling database and fit to a linear regression line with equation $\dot{m}_\mathrm{a} = 0.0036\,wd$. *b)* Channel width variation as a function of the mean thruster diameter for a sample set of low and medium power HETs. The designed thruster is indicated by a red marker. and a linear regression line fits the data to a $w = 0.2172\,d$ relationship.

TABLE I: Thruster Design Parameters

Parameter, Symbol	**Value**
Power, P_in	50 W
Thrust, T	2 mN
Mass flow rate, $\dot{m}$	1 mg/s
Specific Impulse, I_sp	1250 s
Anode discharge voltage, V_d	300 V
Channel length, L	27 mm
Channel width, w	6 mm
Channel mean diameter, D_av	26 mm

regimes; the magnetic field intensity must increase to compensate for smaller thruster dimensions. Understanding the role of the magnetic field in increasing energy efficiency for low-power thrusters is an area of active research [2] [3]. The trade-off between needing to ensure low ion magnetisation and the diminishing of ion wall losses required careful consideration. Currently used models do not take these multiple effects into account and rely on extrapolated scaling laws from medium-sized HETs [25].

The scaled dimensions for the thruster are summarised in Table I.

C. Mechanical Design

Along with the input design parameters, two key considerations must be taken: the design envelope allowed for the thruster and the feasibility of mechanical construction.

While nanosatellite EP systems must work within the standardised volumetic and mass constraints, this project has extraneous specific requirements imposed by the torsional thrust stand used to obtain thrust measurements. The design envelope for the artefact thruster was limited to $40\mathrm{mm} \times 40\mathrm{mm}$ based on the space available on the torsional arm used for the evaluation. A mass limit of $500\mathrm{g}$ was established to mitigate the potential for hysteresis in the flexure bearing and the influence of parasitic forces. These considerations are discussed in detail in Section IV-B2 and differ from the general standards electric thrusters must meet for in-space applications.

The mechanical construction limited the design to parts that can be readily made within the means of the project. A discussion of material selection and manufacturing limitations is included in Section IV.

D. Magnetic Field Design

The magnetic field strength, $\vec{B}$, has a significant influence on the thruster geometry due to its intrinsic relationship with channel length. As introduced in Section III-A, the magnetic field plays a critical role in thruster operation. There are two key functions that the magnetic field must serve:

1) To provide the magnetic component for generating an azimuthal $\vec{E} \times \vec{B}$ field.
2) To reduce the axial mobility of electrons travelling towards the anode.

Electrons from the cathode are subject to an azimuthal drift as a result of the crossed radial magnetic field and the axial electric field. The requirement for the first function arises from the dependence of the neutral-electron collision rate on the axial electron mobility. Electrons travelling from the cathode to the anode undergo ionising collisions with neutral propellant atoms injected into the channel through the anode. Therefore, the magnetic field must be configured so that it is strong enough to capture low-mass electrons but weak enough that it does not affect the high-mass ion trajectories significantly.

The second function requires that the magnetic field be radially aligned with the thruster. The strength of the magnetic field is determined by the magnet selection. The configuration of the magnetic field affects its strength in different regions of the thruster, and thus the thruster's performance. Ideally, the theoretical maximum magnetic field strength should be localised in the vicinity of the exhaust end of the channel, and minimum at the anode end of the channel. Three configurations were simulated as different combinations of N45 magnets and mild steel rods. Configuration 1 showed the best results, containing only N45 magnets. The results do show that

the steel rods can be used to varying the axial distribution of the magnetic field.

Neodymium permanent magnets were selected to generate the magnetic field. Electromagnets (solenoids) were considered as an alternative magnetic field source, but were ruled out as a result of the associated increase in power consumption, heat generation, and design complexity. Initially, a coaxial double-ring permanent magnet configuration following [26] was considered, but there were no commercially available permanent magnets that would fit the small-scale design envelope. Instead, cylindrical, axially magnetised neodymium N45 [10] magnets, and a 1010 mild steel shunt plate were used to create the "revolver" formation of magnets shown in Fig. 8. Stronger permanent magnets were considered, but project budget and limited commercial options narrowed the selection to N45 or lower neodymium magnets. Samarium magnets were considered as an alternative permanent magnet because of their higher temperature tolerances [3], but were discounted due to their weaker magnetic fields.

This assembly is less massive than a cylindrical magnet assembly (since there is less total magnet mass), and it ensures that magnets can be replaced easily and swapped with mild steel cylinders to generate magnetic circuits with different properties for parametric sweeps during testing. The N45 magnets provide an outward radial magnetic field, $\vec{B}$ (shown as blue lines in Fig. 3) and the mild steel shunt plate forms a ground for the magnetic circuit. This ensures that the magnetic field strength through the anode end of the chamber is as low as possible. Note that the magnets must be arranged with the polarisation shown in Fig. 3 to correctly generate the outward radial magnetic field. Since the magnetic field must be perpendicular to the electric field, incorrect placement of the magnets would result in a magnetic field directed in the wrong way, preventing the thruster from operating.

A finite element analysis (FEA) simulation performed on Finite Element Method Magnetics (FEMM)[11] confirmed that the arrangement of the magnets would provide the desired magnetic field. Fig. 5 shows the result of simulating the N45 magnet configuration in FEMM. The magnetic field strength results were plotted as a function of distance down the thruster's channel, producing Fig. 6. These results confirm that the magnetic subsystem could produce the desired magnetic field, with a maximum of 300 mT at the channel exit and a minimum near the anode/shunt plate end of the thruster's 19 mm long chamber.

A Hall-effect probe was used to verify the magnetic configuration. An azmuthially uniform magnetic field strength of 159 mT was measured at the exit of the chamber. Although this is only just over half of the magnetic field strength in the simulation, the polarisation and structure of the magnetic field were confirmed to be correct. One possible explanation for the disagreement in simulated and measured magnetic fields could be that the magnets were exposed to temperatures in excess of their Curie point[12]; the temperature at which they rapidly lose magnetic properties. Another explanation for the loss of magnetisation at the end of the channel could also be oversaturation of the mild steel shunt plate.

[10] '45' denotes the strength of the field produced by the magnet. Higher numbers indicate a stronger magnet

[11] FEMM is an open-source magnetic simulation software.

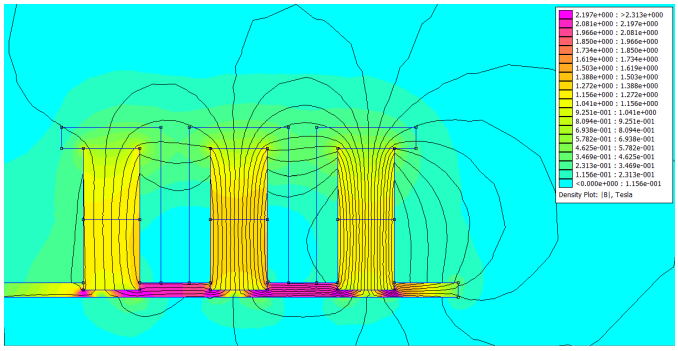

Fig. 5: Resultant magnetic field density plot from FEMM simulation

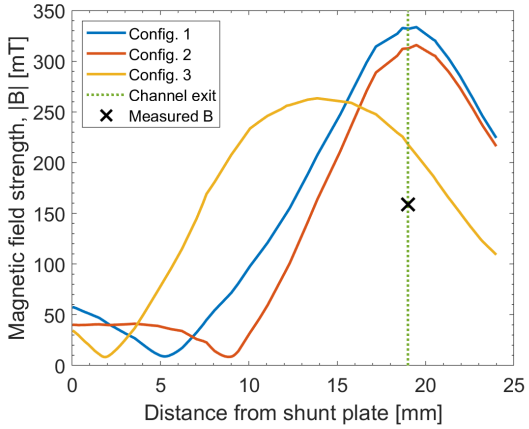

Fig. 6: FEMM simulation results for magnetic field strength plotted as a function of distance down the thruster's channel with three different magnetic configurations. The red dotted line on the figure indicates the position of the channel exit relative to the anode.

E. Thruster Body & Electric Circuit Design

The thruster's body is based on an annular design which is common across HETs of all scales [7] [1]. The main components are the copper anode and the boron nitride insulator which forms the thruster's annular channel.

The electric field, $\vec{E}$ (shown as green lines in Fig. 3), is mostly concentrated at the channel exit, serving two purposes. The first is to drive the Hall current, and the second is to accelerate ions out of the channel, the mechanism which generates thrust. The electric field is generated between the negative potential (created at the end of the thruster chamber by electrons circulating azimuthally along the magnetic field lines) and the positively biased copper anode enclosed by the chamber.

[12] The measurement was taken after several hours of testing, by which the magnets were exposed to temperatures nearing their Curie point.

The thruster channel insulator that contains the plasma discharge was made of boron nitride, a high temperature ceramic [10]. Boron nitride is an excellent thermal insulator that is commonly selected in literature over alternative dielectrics such as alumina due to its low thermal expansion and low erosion rate [19] [26] [14]. These properties allow the channel to maintain a long lifetime while insulating other components (like the permanent magnets) from the higher temperatures associated with plasma discharge.

2 millimetre holes drilled into the anode allow for neutral propellant flow into the chamber. Another design consideration is that an even flow of propellant is required so that maximum performance can be obtained. Several other studies consider complex anode designs that integrate propellant diffusers [24]. A perpendicular inflow through the anode was decided since the diffusivity in supersonic flows would render a more complex diffuser design redundant [13].

F. Hollow Cathode Design

HETs require an electron discharge to ionise neutral propellant gas to create a plasma and to neutralise the ion beam exiting the thruster axially (to ensure maximum momentum transfer from the ions to the thruster [7]).

The properties of the emitter material, the physical configuration, and the structure of the plasma it produces determine the performance and the lifetime of a hollow cathode. The thruster employs an externally mounted low-power heaterless hollow cathode as its electron source. It consists of three key components that each provide a different function: a lanthanum hexaboride ($\mathrm{LaB_6}$) electron-emitting insert, a tantalum cathode tube that holds the insert, and a titanium keeper that facilitates turning on the cathode discharge.

This discharge (often called a plume) is shown in Fig. 15 *a)* and *b)* where blue/purple streams of ions and electrons can be seen leaving the cathode. The plume is nominally consistent during operation, but instabilities in operation replace the stable plume with sparking and sputtering[14], as shown in Fig. 16 *b)*. The keeper is biased positive relative to the cathode tube to initiate Joule heating[15]. Once the insert inside the tip of the cathode tube reaches a sufficient temperature, the $\mathrm{LaB_6}$ begins to thermionically emit electrons, a process governed by the Richardson-Dushman equation [27]:

$$J = A\,T^2\,e^{\frac{\phi_0}{k\,T}}, \tag{13}$$

where J is current density, A is the constant of thermionic emission ($120\,\mathrm{A/cm^2K^2}$), T is the temperature of the emitter, e is the elementary charge, ϕ_0 is the material's work function (which informs the amount of energy required for a material to thermionically emit), and k is the Boltzmann constant ($8.62 \times 10^{-5}\,\mathrm{eV/K}$). Paschen's law gives the breakdown voltage required to ignite plasma, which is a function of the cathode tube-keeper pressure and the type of gas used [28].

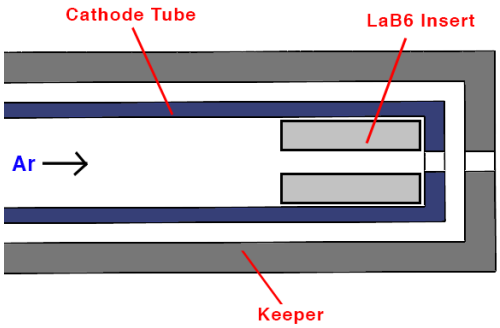

Fig. 7: Cross-sectional view of a the hollow cathode with argon gas injected into the main internal plasma region inside the LaB6 insert.

Typical hollow cathodes use a heater to warm the cathode tube to the required temperature for thermionic emission while minimising cathode degradation [7]. Despite their merits, cathode heaters require a standalone power supply for operation and add mass to the cathode assembly. A heaterless cathode was selected owing to the low mass and power budgets for the thruster.

While heaterless hollow cathodes encounter non-trivial complications such as cathode erosion, runaway thermal problems, and plasma instabilities, they also consume less electrical power and often enable faster thruster ignitions [7] [29]. The electrical characterisation of the hollow cathode allowed for the identification of a stable operating regime, intended to mitigate discharge instabilities and lifetime concerns. The identified test procedure is discussed in Section IV.

The cathode tube should be long and thin to reduce the conductive heat losses, which lowers the requisite power for heating. A Macor[16] ring was fabricated to insulate the negatively biased cathode tube from the positively biased keeper. The interior clearance between the tip of the cathode tube and the keeper was sized at 1 millimetre to ensure that the local neutral gas pressure was sufficiently high for plasma ignition[17]. Tantalum is an expensive, highly conductive element with an extremely high melting point. Its properties necessitate its use for hollow cathode applications, despite the cost. This is reflected in its wide and successful usage in the literature [7] [20] [1]. The keeper electrode must be made from an extremely strong and electrically conductive material to reduce the rate of erosion caused by ion bombardment and high temperatures. The keeper was made of titanium, which exhibits these properties.

$\mathrm{LaB_6}$ is an advantageous material for increased cathode emission due to its low work function and resistance to impurities and air exposure [7]. A low work function means that a material emits electrons at lower temperatures than materials with high work functions, as described in (13)

[13]This decision was based on information discussed with my project supervisors.

[14]Sputtering is a phenomenon where microscopic particles are ejected from the surface of a solid material as a result of its bombardment by energetic particles of a plasma or gas [7].

[15]Joule heating (also known as Ohmic heating) describes the process whereby the energy of an electric current is converted into heat as it flows through a resistance [7].

[16]Macor is a glass-ceramic which is machinable with standard metalworking tools and is a good thermal insulator with low outgassing rates.

[17]The neutral gas pressure inside the hollow cathode affects the plasma density and plasma profile due to collisional effects [7].

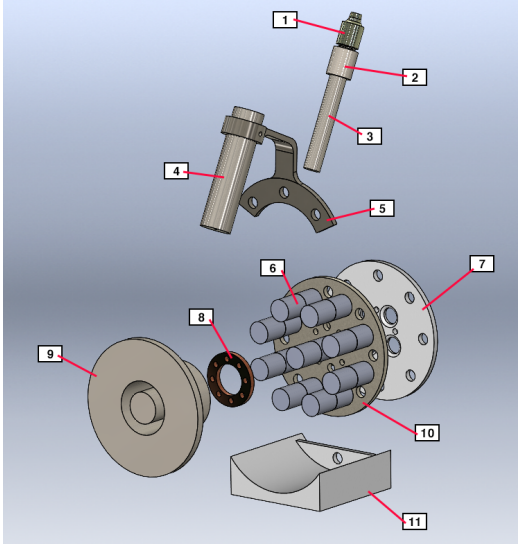

Part	Description
1	Stainless steel propellant connector
2	Alumnia insulator
3	Tantalum cathode tube
4	Titanium retainer
5	Stainless steel bracket
6	Neodymium N45 magnets
7	Boron nitride back insulator
8	Copper anode
9	Boron nitride channel insulator
10	Mild steel shunt plate
11	PTFE (Teflon) stand

Fig. 8: Exploded View of the thruster assembly

[7] [20]. Therefore, low-work function materials require less current through the cathode tube, thus reducing the power they require for operation. It also means that less heat is propagated through the assembly. Other emitter materials, such as barium or alumina oxides (BaO–W), are notably brittle and rapidly degrade inside the hollow cathode, limiting the operational lifetime of the thruster. Furthermore, LaB_6 is significantly less sensitive to impurities and exposure to air than other cathode materials, making it significantly easier to handle in the laboratory environment [7].

IV. Fabrication, Testing & Experimental Apparatus

Fabrication techniques, materials, experimental apparatus, and instrumentation were selected for this project based on their relative merits from applications reported in the literature [2] [10] [1].

A. Fabrication

1) Mechanical, Material & Thermal Considerations: An exploded view of the thruster is shown in Fig. 8 with its materials labelled. Mechanical construction was informed by three key factors: scaled dimensions, magnetic field topology, and material considerations. The materials, off-the-shelf components, and fixtures used for this project had to be considered in terms of the properties listed below.

1) Electrical conductivity: while parts such as the anode, cathode, and keeper had to be electrically charged, other parts such as the ceramic backplate served as insulators to prevent electrical shorts.
2) Thermal conductivity: thermally insulating materials were used in this project to prevent the propagation of heat through the system. The significant thermal strain the cathode places on the system requires special consideration on the thermodynamic properties of materials, such as their thermal expansion coefficients and thermal conductivity. The goal with thermal design is to protect heat-sensitive components from overheating.
3) Magnetic permeability and coercivity: cylindrical magnets had to have sufficient magnetic properties to enable the operation of the magnetic circuit, and the mild steel shunt plate had to be thick enough to prevent its saturation in the magnetic circuit, without adding excessive mass.
4) Low cost: parts had to be procured within the limited budget allocated to the project: materials had to show low outgassing rates to be used in the vacuum chamber (this was assessed by consulting with technical staff at RRI).
5) Tolerant of thermal stresses: the temperatures around the thruster reached temperatures in the hundreds of degrees Celsius; thus, all components had to tolerate thermal stresses. Parts of the hollow cathode assembly reached temperatures near $1000\,^{\circ}\mathrm{C}$.
6) Safe to use: components had to be safe to handle and had to meet the safety requirements set by New Zealand laboratory standards.

2) Propellant Delivery: Propellant was delivered from a gas storage tank to two mass flow controllers outside the vacuum chamber through 1/4 inch steel tubing. The mass flow controllers communicated over the network to enable centralised LabVIEW control of propellant to the cathode and anode. The cathode and anode lines connected to a central manifold block inside the vacuum chamber via a feedthrough connection on the chamber wall. Press-fit silicon propellant lines were used to deliver argon gas from the manifold to both the cathode and anode. The anode connection was split into four using a custom cylindrical stainless steel propellant manifold. The manifold and anode were designed to increase the overall uniformity of the propellant flow in the thruster channel. The distribution of propellant in the channel should be isotropic to achieve the maximum rate of ionisation rate, ergo maximum thrust. However, this is difficult to guarantee.

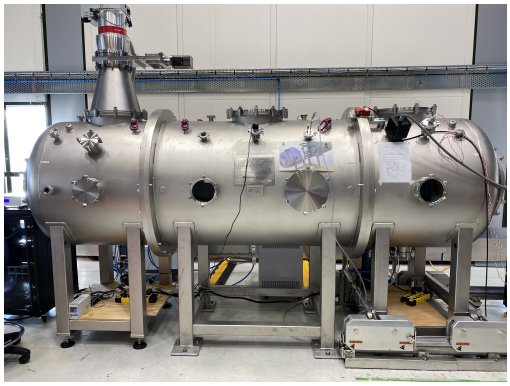

Fig. 9: The large vaccum chamber at RRI.

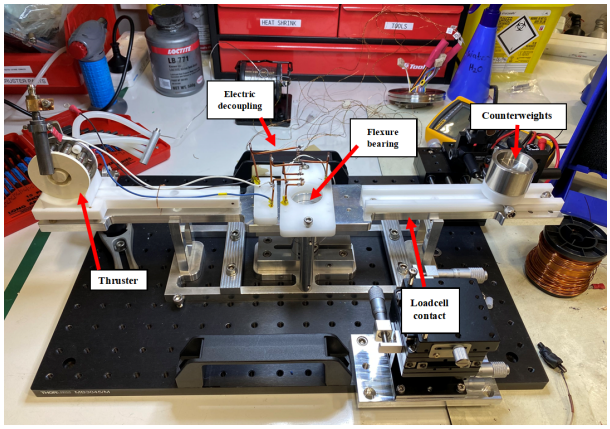

Fig. 10: Torsional thrust stand with key components labelled

B. Testing Facilities and Instrumentation

Accurate ground testing of electric thrusters is crucial to understanding how such devices will behave in space [30]. Identifying and mitigating potential failure points during ground tests minimises the probability of failure after launch, supporting sustainable space exploration. Furthermore, evaluating the performance of EP devices in ground testing facilities is essential for the iterative design process, which is synonymous with research and development in aerospace engineering. The key challenge in electric thruster ground testing lies in accurately simulating the space environment (vacuum, cryogenic temperatures, and microgravity) and verifying the thruster's operation by gathering thrust measurements. To draw any valid conclusions on the results gathered during ground testing, the behaviour of the thruster, as well as the influence of dynamic background effects, must be understood.

1) Vacuum Chamber Facility: All tests performed under vacuum conditions were performed at RRI in a $2.75\,\mathrm{m}^3$ vacuum chamber shown in Fig. 9. The vacuum chamber uses a Pfeiffer HiPace 1500 turbo pump, a multistage Pfeiffer roughing pump, and a Trillium CP16 cryogenic vacuum (cryo) pump. The setup at RRI is the largest and most advanced EP testing facility in New Zealand, capable of achieving a background pressure of $\sim 1 \times 10^{-6}\,\mathrm{mbar}$, which decreases to $\sim 1 \times 10^{-4}\,\mathrm{mbar}$ during operation. The vacuum chamber valves, the mass flow rates of the anode and cathode, and power supply unit (PSU) were controlled through a central network device that runs LabVIEW software[18]. The torsional thrust stand load cell was connected through the walls of the vacuum chamber via a DB-15 feedthrough.

2) Instrumentation of Torsional Thrust Stand: Torsional pendulums use a central flexure bearing to allow a twisting motion and counterweights to null self-weight caused by gravity. When fired, the thruster exerts a force on the torsional arm, generating a torque which exerts an (ideally) equal and opposite force on the load cell. This configuration is shown in Fig. 10. The load cell generates a voltage proportional to the force that is reported to the LabVIEW software through a NI data acquisitions (DAQ) device. The DAQ's analogue input module sampled at 100 Hz using a 1 Vpp 24-bit analogue to digital conversion input range. Initial calibration and validation by known mass was performed before and after test conditions were varied to obtain the voltage-force relationship that characterises the load cell's measurements. A characterisation of the thrust stand identified the presence of parasitic forces in the configuration. Such forces counteract the force generated by the thruster and often inflict non-linear and hysteresis effects [31]. These forces were determined to be caused by the ridgity introduced to the pendulum by electrical connections and propellant lines and were amplified by an underdamped torsional system. These forces had to be mitigated to ensure precision and repeatability in thrust measurements. This was done by connecting the thruster's requisite electrical and gas connections to the thrust stand with decoupling points around the axis of rotation. Furthermore, magnets on the torsional arm were introduced to damp parasitic oscillations and preload the load cell. Preloading ensures that a measurement is taken within the load cell's linear behaviour region.

[18]LabVIEW is a systems engineering software for testing and control instrumentation, made by National Instruments (NI).

C. Testing & Results

The parameters of interest for testing included standard performance metrics for electric thrusters, such as power, thrust, specific impulse, and overall efficiency. A parametric sweep identified propellant mass flow rate and current as the key variable test parameters that would provide values to evaluate various performance metrics.

1) Cathode Characterisation: Before a hollow cathode discharge can be initiated, it is necessary to condition the cathode for operation [29]. Conditioning is performed to safely remove contaminants deposited on the emitter during the outgassing of components or during handling in the laboratory. These contaminants increase the work function of the emitter material, meaning that more power is required to heat the cathode to its thermionic temperature. This can lead to thermal runaway effects, severely diminishing cathode lifetime, and potentially damaging thruster components. Conditioning is performed by running the cathode outside of the thruster assembly for several hours, with an external metal target acting as the positive electrode. The cathode required approximately 12 hours of conditioning (shown in Fig. 16 *a.*) before it could be routinely ignited.

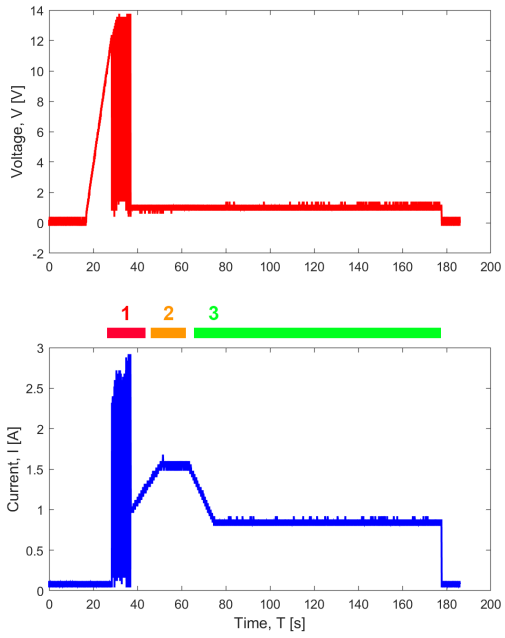

Fig. 11: The three operational stages of the hollow cathode shown in a sample of experimental data, which are: Stage 1) Cathode heating, Stage 2) Plasma ignition, and Stage 3) Stable glow discharge.

The behaviour of the cathode was investigated by varying both the cathode current and the mass flow rate. The cathode ignition process has three main steps:

1) Cathode heating: The cathode current is ramped up to and held at 1.5 A for 10 seconds to allow the cathode's emitter to heat. Argon propellant is injected into the cathode at 6 mg/s.
2) Ignition to thermionic emission: Once the cathode's emitter has heated enough, it will begin to themionically emit, causing sparks and plasma to ignite. The discharge eventually stablises after 10s of seconds.
3) Stable glow discharge: The current is ramped down to a target operating current, I_x, and a mass flow rate $\dot{m}_x$. The test ends after about 100 seconds of operation.

The cathode current and voltage in time measured by an oscilloscope are shown in Fig. 11 where the timestamps for the three operating stages of the cathode are indicated in red, orange, and green. Note the noise present in the voltage and current measurements for the initial heating/ignition stage. The results of the cathode characterisation are summarised in Fig. 12. The relationship between discharge voltage and current that varies with mass flow rate is clearly observable.

2) Anode Operation & Thrust Measurements: Thrust was recorded on the torsional thrust stand, using the set-up described in Section IV-B2. Initial cold gas tests were performed to verify the operations of the load cell and the propellant delivery system. The difference between the raw and post-processed thrust measurements is shown in Fig. 13 *a)*. Post-processing was performed using MATLAB's Curve Fitting

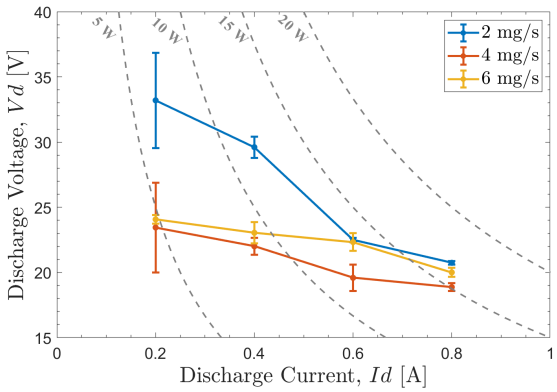

Fig. 12: A summary of results from the characterisation of the hollow cathode, including error bars which were calculated from the standard deviation between repeated measurements for each point.

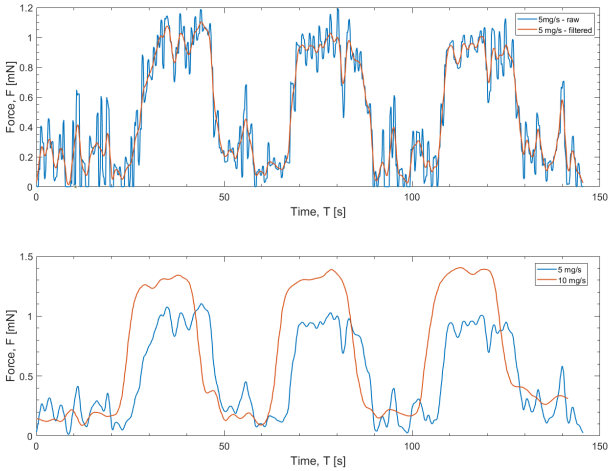

Fig. 13: *a)* A sample cold gas thrust measurement, before and after post-processing. *b)* Thrust measurements taken with 5 mg/s and 10 mg/s of argon gas.

Toolbox, allowing for rapid and streamlined data conditioning. The post-processed data allows for better interpretation of the results while maintaining data integrity. The cold gas test was performed as two tests, one with a mass flow rate of 5 mg/s and the other with 10 mg/s. Each test was run in three on/off cycles. The results are shown in Fig. 13 *b)* and indicate a clear difference between the test with a mass flow rate of 5 mg/s, and the test with 10 mg/s, as well as clear rising and falling edges on the ON/OFF cycles. This verifies the ability of the load cell to capture thrust in time, which is crucial to evaluating HETs. The cold gas test can also be used to verify the thruster's operation; if the measured force is similar to the cold gas test, it is likely that the thruster is not providing additional force, meaning that it is not operating effectively.

Thrust measurements were recorded while the thruster was operated with 6 mg/s propellant to its anode and performing tests over a range of anode currents (0.2 to 1 A). The tests were repeated with an anode mass flow rate of 10 mg/s. Each

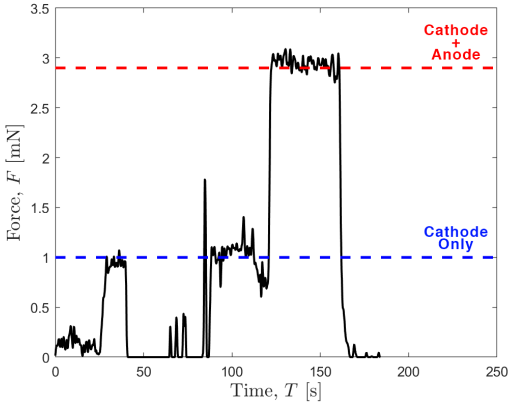

Fig. 14: A thrust measurement from the load cell showing 1 mN of force with the cathode operating alone and almost 3 mN of force generated after the anode power supply was turned on.

individual test started with cathode warm-up and ignition, following the test procedure described in Section IV-C1. Once the cathode reached a stable thermionic discharge mode, the anode power supply and mass flow rate were switched on. Fig. 14 shows the result of a test carried out with an anode current and voltage of 1 A and 80 V, respectively (with a 4 V drop over a 4 Ω resistor is series with PSU). a voltage of 80 V and a mass flow rate of 10 mg/s. The distinction between the cathode's operation and the entire system's operation is clear. The cathode achieved about 1 mN of force, approximately the same thrust measured during the cold gas test with a similar mass flow rate. A clear increase in force on the load cell from 1 mN to almost 3 mN is observed after a short stabilisation period after the anode is switched about 80 seconds into the test. Noise in the thrust measurement is likely caused by the oscillatory behaviour of the flexure bearing. Future tests should consider employing a low-pass filter or increasing the magnetic preload to damp the high-frequency oscillatory modes present in the torsional system.

V. Discussion

A. Cathode Characterisation

The characterisation of the hollow cathode shown in Fig. 12 identifies several stable operating points and the input power required to operate at them. An optimal stable cathode operating regime was identified at $I = 0.6\,\mathrm{A}$ and $\dot{m}_\mathrm{a} = 4\,\mathrm{mg/s}$. In this regime, the cathode could be reliably ignited for several tens of tests. The i^2 relationship current has with power indicates that minimal power savings can be achieved with low mass flow rates when operating at currents greater than 0.6 A. It seems that the optimal solution to this trade-off would be to increase the cathode mass flow rate as much as possible to minimise the current required for stable operation. This solution is correct in principle, but neglects to acknowledge the inversely proportional relationship of efficiency with the mass flow rate, shown in (3). As the current increases, the power saved by using high mass flow rates becomes less worthwhile. A more sensible trade-off is obtained by selecting a stable operating mode under 10 W (which conserves up to 40 W out of the total budgeted 50 W for the main thruster's operation) at the knee of the current-voltage curve, where power falls off steeply with mass flow rate. This operating point was identified as $I = 0.4\,\mathrm{A}$ with $\dot{m}_\mathrm{a} = 4\,\mathrm{mg/s}$.

Fig. 12 also identifies another key pattern; the voltage required for thermionic emission increases steeply at low mass flow rates and low currents, which are the two requisites for low-power thruster operation (as indicated by the power lines drawn in grey). This result makes sense as the plasma ignition depends both on the gas pressure in the cathode and the breakdown voltage, meaning that operation at mass flow rates below 2 mg/s requires the use of significantly higher voltages.

B. Thruster Characterisation

The thrust produced by the thruster exceeded the target of 2 mN, generating up to 4 mN in some tests. A repeatable measurement of 3 mN was achieved with the cathode operating at $I_\mathrm{c} = 0.6\,\mathrm{A}$ and $\dot{m}_\mathrm{c} = 4\,\mathrm{mg/s}$, and the anode operating at $I_\mathrm{a} = 0.2\,\mathrm{A}$ and $\dot{m}_\mathrm{a} = 10\,\mathrm{mg/s}$, as shown in Fig. 14.

Although the thruster operated with mass flow rates exceeding the target value (less than 1 mg/s), the results of testing successfully demonstrate the stable operation of a low power HET. High mass flow rates overwhelmed the vacuum chamber pumping equipment, meaning that the chamber temperature and pressure were an order of magnitude higher than usual. The implication of these conditions was that stable plasma ignition could not be maintained for long durations.

The 150 V power supply used during testing prevented high anode discharge voltages from being realised. There is agreement between the literature [7] [28] and the cathode charcterisation results on the limits that low discharge voltages impose on thruster efficiency. Should a higher voltage supply be employed, lower mass flow rates and higher exhaust velocities could be realised, thus increasing thruster specific impulse/efficiency. Therefore, a higher voltage power supply is recommended for the anode power supply in future characterisation.

C. Performance

The thruster's performance can be evaluated against three core metrics: thrust, specific impulse, and efficiency, which were derived with (1)-(3). The thruster can achieve 3 mN of thrust, which corresponds to an exhaust velocity of 214 m/s and a specific impulse of 21.85 s. The thruster consumes 50 W of power with an overall efficiency of less than 1 %. These results were compared to a 52 W reference thruster from the literature [19], which achieved 2.6 mN of thrust with a specific impulse of 817 s and overall efficiency of 20%. The reference thruster had a discharge voltage exceeding 250 V, and demonstrated the requirement for high voltages to generate thrust effectively. Despite the comparably low efficiency and specific impulse of the developed thruster, the 2 mN thrust target set by the VUW CubeSat mission was exceeded while operating within the 50 W target power regime. This indicates significant potential for further development and optimisation.

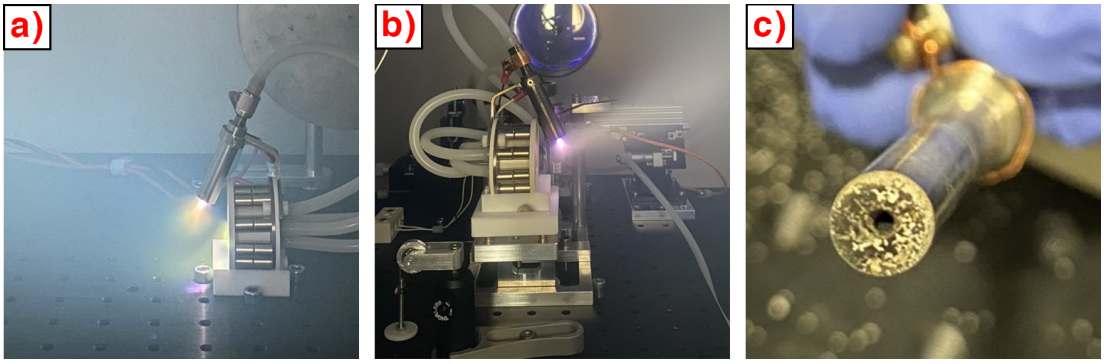

Fig. 15: *a)* Example of stable cathode operation. *b)* Stable cathode operation on thrust stand. *c)* Cathode wear after about 50 hours of testing

D. Stability & Reliability

Although the cathode could successfully ignite with mass flow rates as low as 0.5 mg/s, resultant thermal issues disallowed steady-state operation in this regime, ergo the cathode's behaviour in this regime could not be characterised. During these low mass flow rate tests, the plasma discharge would become highly unstable [19], whereby the cathode would rapidly overheat (causing the cathode keeper to glow bright orange).

This observed thermal runaway effect resulted in contamination of the LaB_6 emitter, causing the cathode's operation to become unstable over all testing regimes. This is a documented problem associated with emitter materials in hollow cathodes [7] [29]. The solution is generally to follow the conditioning process described in Section IV-C1. Although this reconditioning successfully removed the impurities on the LaB_6 emitter, the problem's occurrence highlights a greater issue pertinent to HETs; ensuring cathode lifetime.

Instabilities in the plasma discharge of the thruster and its hollow cathode were observed. These were likely the result of operating at the incorrect voltage or current, or were also an observable consequence of significant overheating, incorrect operating parameters. Induced by rapidly changing conditions inside the cathode, these fluctuations have been reported to produce extremely high-energy ions that accelerate cathode keeper and ionisation channel erosion [7] [29]. This has been identified as a major cause of HET failure in space [32], which, given the increased thermal stresses on small-scale thrusters (owing to smaller radiative energy transfer areas), poses a crucial problem to be addressed by future miniaturised thruster development. This work may require a thermal analysis of the current cathode assembly to identify the salient causes of plasma instabilities in the cathode.

E. Electromagnetic Interference

The thruster showed a tendency to produce electromagnetic noise during testing. Electromagnetic interference can affect spacecraft communications and payload functionality [2]. The effect of this noise on test instrumentation and external electronics necessitates further interference characterisation and compatibility testing before the thruster can be used on the proposed 3U CubeSat.

[19]Instabilities in the cathode's discharge were observed quantitatively on the oscilloscope, and visually through the vacuum chamber's window by examining the cathode's plume.

VI. Conclusions and Future Work

A low-power Hall-effect thruster was developed and evaluated quantitatively with thrust measurements from a torsional thrust stand, as shown in Fig. 16 *c)*. The 50 W thruster was shown to produce 3 mN of thrust and 28.75 s of specific impulse. The collected thrust measurements serve as foundational data for subsequent design iterations. A comparison between the developed thruster and a similar low-power thruster from the literature indicates that the thruster's low efficiency could be caused by an insufficiently high discharge voltage, identifying a clear avenue for future investigation. The presented thruster achieved thrust exceeding the 2 mN required by the proposed VUW orbit-raising mission, and can operate within the target power regime of 50 W. These results suggest that future iterations may be able to support the ambitious mission proposed by VUW.

This paper also presented an expeditious semi-empirical scaling and design methodology for low-power EP thrusters. This methodology was shown to be a powerful tool enabling the rapid and accurate estimation of thruster performance characteristics and dimensions, which is congruous with today's age of accelerated satellite deployment and space exploration.

This study identified the magnetic field strength as a significant parameter of influence on thruster performance. Characterisation of the various magnetic configurations available with this thruster assembly was outside the scope of this project, but should be a key focus of future work, especially exploring the role magnetic field uniformity down the channel plays in the mechanisms of ion acceleration. Furthermore, new magnet types should be investigated as well as the potential application of superconducting magnets to generate very strong magnetic fields. Superconducting materials have already been identified as a salient point of future research in the field of electric propulsion [33] [2].

EP literature distinctly lacks comprehensive studies on the design and testing of miniaturised HETs. This places an inherent value on the results observed in this study. The project goals identified in Section I have all been met: a suitable thruster technology was identified, the underlying

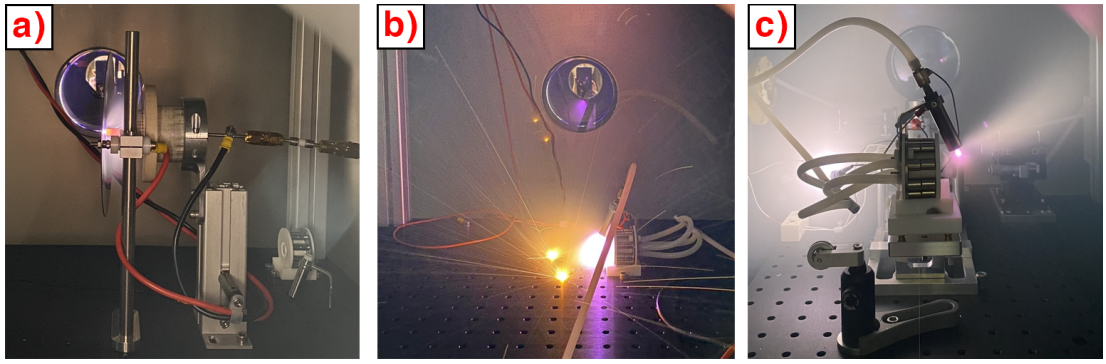

Fig. 16: *a)* Conditioning outside of the thruster assembly performed with an external metal target. *b)* Unstable cathode operation. *c)* Stable thruster operation on torsional thrust stand with an extraneous plasma ignited on an exposed wire in the background

physics behind the thruster's key sub-systems were explored, a mechanical design for the thruster was produced using CAD modelling and FEA, and successful operation of the thruster was demonstrated, with characteristic testing results shared and discussed.

The success of this project marks a significant step towards the realisation of advanced satellite manoeuvres for small-scale academic space projects and the sustainable exploration of space.

REFERENCES

[1] I. Levchenko, K. Bazaka, Y. Ding, Y. Raitses, S. Mazouffre, T. Henning, P. J. Klar, S. Shinohara, J. Schein, L. Garrigues, *et al.*, "Space micropropulsion systems for cubesats and small satellites: From proximate targets to furthermost frontiers," *Applied Physics Reviews*, vol. 5, no. 1, 2018.

[2] NASA, "State-of-the-art of small spacecraft technology," Tech. Rep. TP—2022–0018058, Small Spacecraft Systems Virtual Institute, Ames Research Center, Moffett Field, California, January 2022.

[3] S. Mazouffre, "Electric propulsion for satellites and spacecraft: established technologies and novel approaches," *Plasma Sources Science and Technology*, vol. 25, no. 3, 2016.

[4] Z. Jaeger-Letts, J. Glowacki, and C. Hollitt, "Mission design and analysis of an electric propulsion nanosatellite mission." 2022.

[5] M. Grande, L. Guo, and M. Blanc, "Chapter 5 - enabling technologies for planetary exploration," in *Planetary Exploration Horizon 2061*, pp. 249–329, Elsevier, 2023.

[6] I. Levchenko, S. Xu, S. Mazouffre, D. Lev, D. Pedrini, D. Goebel, L. Garrigues, F. Taccogna, and K. Bazaka, "Perspectives, frontiers, and new horizons for plasma-based space electric propulsion," *Physics of Plasmas*, vol. 27, no. 2, 2020.

[7] D. Goebel and I. Katz, *Fundamentals of Electric Propulsion: Ion and Hall Thrusters*. JPL Space Science and Technology Series, Wiley, 2008.

[8] R. G. Jahn, "Electric propulsion," *American Scientist*, vol. 52, no. 2, pp. 207–217, 1964.

[9] E. Tsiolkovsky, "Investigation of universal space by means of reactive devices," 1903.

[10] M. Baird, "Designing an accessible hall effect thruster," bachelor's thesis, 2016.

[11] NASA, "Space debris and human spacecraft." https://www.nasa.gov/mission_pages/station/news/orbital_debris.html, 2021. Accessed: 2023-06-01.

[12] G. P. Sutton and O. Biblarz, *Rocket propulsion elements*. John Wiley & Sons, 2016.

[13] T. Pultarova, "Hydrazine ban could cost europe's space industry billions," Feb 2023.

[14] D. Krejci and P. Lozano, "Space propulsion technology for small spacecraft," *Proceedings of the IEEE*, vol. 106, no. 3, pp. 362–378, 2018.

[15] M. Peukert and B. Wollenhaupt, "Ohb-system's view on electric propulsion needs," tech. rep., 2014.

[16] D. Lev, R. M. Myers, K. M. Lemmer, J. Kolbeck, H. Koizumi, and K. Polzin, "The technological and commercial expansion of electric propulsion," *Acta Astronautica*, vol. 159, pp. 213–227, 2019.

[17] D. Zolotukhin, A. Tyunkov, Y. G. Yushkov, S. Bandaru, K. Daniels, and M. Keidar, "A two-stage μcat-mpd thruster: toward millinewton thrust," *Journal of Electric Propulsion*, vol. 1, no. 1, p. 22, 2022.

[18] H. Watanabe, S. Cho, and K. Kubota, "Performance and plume characteristics of an 85 w class hall thruster," *Acta Astronautica*, vol. 166, pp. 227–237, 2020.

[19] D. Lee, H. Kim, S. Lee, G. Doh, and W. Choe, "Development and performance test of a 50 w-class hall thruster," in *36th International Electric Propulsion Conference (University of Vienna, Vienna, Austria*, pp. 15–20, 2019.

[20] F. Nürmberger, A. Hock, and M. Tajmar, "Design and experimental investigation of a low-power hall effect thruster and a low-current hollow cathode," *AIAA Paper*, vol. 3822, p. 2015, 2015.

[21] K. Dannenmayer and S. Mazouffre, "Elementary scaling relations for hall effect thrusters," *Journal of Propulsion and Power*, vol. 27, no. 1, pp. 236–245, 2011.

[22] J. Ashkenazy, Y. Raitses, and G. Appelbaum, "Low power scaling of hall thrusters," in *European Spacecraft Propulsion Conference*, vol. 398, p. 455, 1997.

[23] M. Andrenucci, L. Biagioni, S. Marcuccio, and F. Paganucci, "Fundamental scaling laws for electric propulsion concepts," in *28th International Electric Propulsion Conference*, p. 1721, 2003.

[24] B. Oh, A. Countryman, M. Regassa, A. Clowes, G. Miner, S. Kemp, S. cAneney, M. Klein, and C. Lee, "Design, fabrication, and testing of an undergraduate hall effect thruster," *Journal of Electric Propulsion*, vol. 2, no. 1, p. 6, 2023.

[25] E. Lee, Y. Kim, H. Lee, H. Kim, G. Doh, D. Lee, and W. Choe, "Scaling approach for sub-kilowatt hall-effect thrusters," *Journal of Propulsion and Power*, vol. 35, no. 6, pp. 1073–1079, 2019.

[26] Y. Ding, H. Sun, W. Peng, Y. Xu, L. Wei, H. Li, P. Li, H. Su, and D. Yu, "Experimental test of 200 w hall thruster with titanium wall," *Japanese Journal of Applied Physics*, vol. 56, no. 5, p. 050312, 2017.

[27] D. M. Goebel, G. Becatti, I. G. Mikellides, and A. Lopez Ortega, "Plasma hollow cathodes," *Journal of Applied Physics*, vol. 130, no. 5, 2021.

[28] H. Eichhorn, K. Schoenbach, and T. Tessnow, "Paschen's law for a hollow cathode discharge," *Applied physics letters*, vol. 63, no. 18, pp. 2481–2483, 1993.

[29] B. Rubin and J. D. Williams, "Hollow cathode conditioning and discharge initiation," *Journal of Applied Physics*, vol. 104, no. 5, 2008.

[30] T. Randolph, V. Kim, H. Kaufman, K. Kozubsky, V. Zhurin, and M. Day, "Facility effects on stationary plasma thruster testing," in *23rd International Electric Propulsion Conference*, no. 844, pp. 13–16, The Electric Rocket Propulsion Society Worthington, OH, 1993.

[31] E. Webster and J. Głowacki, "Micro thrust stand commissioning report – rri endeavour pg3," tech. rep., 2022.

[32] A. Sengupta, J. Brophy, J. Anderson, C. Garner, B. Banks, and K. Groh, "An overview of the results from the 30,000 hr life test of deep space 1 flight spare ion engine," in *40th AIAA/ASME/SAE/ASEE Joint Propulsion Conference and Exhibit*, p. 3608, 2004.

[33] G. Guerrini, C. Michaut, M. Dudeck, and M. Bacal, "Parameter analysis of three ion thrusters (spt-20, spt-50 and a-3)," in *European Spacecraft Propulsion Conference*, vol. 398, p. 441, 1997.